New line intensity measurements for 12C2H2 around 7.7 μm and HITRAN format line list for applications

Laura Gomez, David Jacquemart, Nelly Lacome, Jean-Yves Mandin

New line intensity measurements for $^{12}C_2H_2$ around 7.7 µm and HITRAN format line list for applications

L. Gomez [a,b], D. Jacquemart [a,b,*], N. Lacome [a,b], J.-Y. Mandin [c,d]

[a] *UPMC Univ Paris 06, UMR 7075, Laboratoire de Dynamique Interactions et Réactivité, Case courrier 49, Bât. F 74, 4, place Jussieu, 75252 Paris Cedex 05, France*

[b] *CNRS, UMR 7075, Laboratoire de Dynamique Interactions et Réactivité, Case courrier 49, Bât. F 74, 4, place Jussieu, 75252 Paris Cedex 05, France*

[c] *UPMC Univ Paris 06, UMR 7092, Laboratoire de Physique Moléculaire pour l'Atmosphère et l'Astrophysique, Case courrier 76, 4, place Jussieu, 75252 Paris Cedex 05, France*

[d] *CNRS, UMR 7092, Laboratoire de Physique Moléculaire pour l'Atmosphère et l'Astrophysique, Case courrier 76, 4, place Jussieu, 75252 Paris Cedex 05, France*

****

Version du 25/06/2009

Avant soumission: **-** updater les **** et les lists of captions,
- updater le Supplementary material.

****

[*] Corresponding author at : UPMC Univ Paris 06, UMR 7075, Laboratoire de Dynamique Interactions et Réactivité, Case courrier 49, Bât. F 74, 4, place Jussieu, 75252 Paris Cedex 05, France. Tel.: + 33 1 44 27 36 82; fax: + 33 1 44 27 30 21.

E-mail address: david.jacquemart@upmc.fr (D. Jacquemart).

ABSTRACT

Absolute intensities of 467 lines are measured in 9 bands of the 7.7 µm spectral region of the $^{12}C_2H_2$ molecule, with an average accuracy of 5%. For each band, the vibrational transition dipole moment squared and Herman-Wallis coefficients are obtained in order to model the rotational dependence of the transition dipole moment squared. These results are used to calculate a line list for atmospheric or astrophysical applications. Merged in the line list set up in a previous work for the 8 strongest bands around 7.7 µm [Gomez et al. Line intensities of $^{12}C_2H_2$ in the 7.7 µm spectral region. JQSRT, in press, http://dx.doi.org/10.1016/j.jqsrt.2009.05.018], these new data give now a quasi-exhaustive view of the $^{12}C_2H_2$ spectrum in the involved spectral region.

Keywords:
Acetylene
Infrared
Vibro-rotational transitions
Line intensities
Databases

1. Introduction

The 7.7 µm spectral region of acetylene $^{12}C_2H_2$ is known mainly since the extensive work of assignment performed by Kabbadj et al. [1] in 1991. As far as line intensities are concerned, accurate absolute values were obtained by Vander Auwera [2] in 2000 for the $(\nu_4 + \nu_5)^0_+$ and $(\nu_4 + \nu_5)^2$ cold bands, and then by Jacquemart et al. [3] and Lepère et al. [4] for the $(\nu_4 + \nu_5)^0_+$ band. A more detailed bibliography has been given in Ref. [5]. This spectral region corresponds to the $\Delta P = 2$ sequence of vibrational transitions [6], P being a pseudo-quantum number equals $5v_1 + 3v_2 + 5v_3 + v_4 + v_5$, where v_1, v_2, v_3, v_4, and v_5 are the quantum numbers associated with the normal modes of vibration of the molecule in the ground electronic state. As the spectral region around 7.7 µm is of interest for astrophysical applications (see, e.g., Ref. [7]), it has been important to increase the knowledge of line intensities in order to improve databases [8,9], which contained data only for the $(\nu_4 + \nu_5)^0_+$ band, issued from Ref. [3]. Thus, in a previous work [5], we measured 414 line intensities in 8 hot bands around 7.7 µm, and set up a line list from these results. In the present paper, we report line intensities obtained in the 9 remaining bands assigned by Kabbadj et al. [1].

The studied bands are gathered in Table 1. We have adopted the same notations as in Ref. [5]. A given value of P is assigned to a given set of interacting vibrational states, named polyad or cluster. Then, polyads are noted $\{P\nu_5\}$. Vibrational levels are noted $v_1\, v_2\, v_3\, (v_4\, v_5)\, ^{\ell}_{\pm}\, r$, with $\ell = |\ell_4 + \ell_5|$, ℓ_t being the vibrational angular momentum quantum number associated with the degenerate bending mode t, $\pm$ being the symmetry type for Σ vibrational states ($\ell = 0$), and r a roman numeral indicating the rank of the level, by decreasing energy value ($r =$ I for the highest energy level), inside the set of states having the same vibrational symmetry, and coupled by ℓ-type resonances. Section 2 of the paper recalls the experimental conditions and the measurement procedure, the data reduction is explained in Section 3, and the last section recalls how we have proceeded to set up a line list for databases.

2. Experimental details and measurement procedure

The 6 spectra used in this work are the same as in Ref. [5]. They have been recorded with the rapid scan Bruker IFS 120 HR interferometer of the LADIR (Laboratoire de Dynamique Interactions et Réactivité) in Paris. The main experimental conditions are gathered in Table 2. The temperature of the gas in the cell was recorded via four platinum probes at different places inside the cell. The uncertainty on the temperature measurements has been estimated to be ±0.5 K. Pressures were measured using two full scale ranges MKS Baratrons (10- and 100-Torr manometers) with an accuracy of 0.5%. More experimental details are given in Section 2 of Ref. [5].

The same multispectrum procedure as in Ref. [5] was used to deduce line intensities from the spectra, following a method already described [10]. A Voigt profile was used to calculate the absorption coefficient of the lines, the Doppler-width being kept fixed at its theoretical value, and the baseline is adjusted as a polynomial of the second degree around each studied line. Because of the relatively low pressures, the self-broadening coefficients were fixed at the values calculated according to Ref. [11], and the self-shifting coefficients were fixed at zero. Finally, 467 line intensities have been measured in 9 bands with an average accuracy estimated around 5%. Note that the uncertainty can attain 10% or more for weak lines or overlapped ones.

Results obtained for selected bands are given in Table 3. The full list of results is given in Supplementary material.

3. Data reduction

Let us recall the equations needed to reduce experimental data. For each line intensity $S(T_0)$ obtained from the multispectrum fitting procedure, in cm molecule^{-1} for pure $^{12}C_2H_2$ (i.e., for a sample containing 100% of $^{12}C_2H_2$) at the standard temperature T_0 = 296 K, we use the following formula to deduce the transition dipole moment squared $|R|^2$, in D^2 (1 debye = 3.33546 × 10^{-30} C m)

$$S(T_0) = (1/4\pi\varepsilon_0)\,(8\pi^3/3hc)\,[g''\nu_0\,/\,g_V\,Q(T_0)]\,|R|^2\,L(J,\ell)\,\exp(-hcE''/kT_0)\,[1-\exp(-hc\nu_0/kT_0)], \quad (1)$$

where $1/4\pi\varepsilon_0 = 10^{-36}$ erg cm^3 D^{-2}; h is Planck's constant equal to 6.6260755 × 10^{-27} erg s (1 erg = 10^{-7} J); c is the speed of light in vacuum equal to 2.99792458 × 10^{10} cm s^{-1}; g'' is the statistical weight due to nuclear spin of the lower level (1 for *s*-type levels and 3 for *a*-type levels); ν_0 is the transition wavenumber in cm^{-1}; g_V depends on the degeneracy of the levels involved, with the convention g_V equalling 2 if both upper and lower vibrational states are degenerate and equalling 1 otherwise; $Q(T_0)$ is the total partition function at temperature T_0, calculated from Fischer et al. [12]; $L(J,\ell)$ is the Hönl-London factor; E'', in cm^{-1}, is the energy of the lower level taken from HITRAN [8]; k is Boltzmann's constant equal to 1.380658 × 10^{-16} erg K^{-1}.

Among the 9 studied bands, 8 are parallel ones (4 of them being ℓ-type doubled) and one is a perpendicular band with a *Q*-branch. For *P*- and *R*-branches of parallel bands ($\Delta\ell = 0$), the Hönl-London factor is, vs. ℓ and the rotational quantum number J of the lower level of the transition

$$L(J,\ell) = (J+1+\ell)\,(J+1-\ell)\,/\,(J+1) \text{ (for } R\text{-branch)}, \quad (2)$$

$$L(J,\ell) = (J+\ell)\,(J-\ell)\,/\,J \text{ (for } P\text{-branch)}. \quad (3)$$

For the perpendicular band ($\Delta\ell = \pm1$), the Hönl-London factor is

$$L(J,\ell) = (J+2+\ell\Delta\ell)\,(J+1+\ell\Delta\ell)\,/\,[2(J+1)] \text{ (for } R\text{-branch)}, \quad (4)$$

$$L(J,\ell) = (J+1+\ell\Delta\ell)\,(J-\ell\Delta\ell)\,(2J+1)\,/\,[2J(J+1)] \text{ (for } Q\text{-branch)}, \quad (5)$$

$$L(J,\ell) = (J-1-\ell\Delta\ell)\,(J-\ell\Delta\ell)\,/\,(2J) \text{ (for } P\text{-branch)}. \quad (6)$$

To reduce the data, effective parameters can be deduced expanding $|R|^2$ to take into account the rotational dependence and possible resonances. For the studied bands, the following Herman-Wallis-type factors have been used

$$|R|^2 = |R_0|^2\,[1 + A_1^{PR}\,m + A_2^{PR}\,m^2]^2 \text{ (for } P\text{- and } R\text{-branches)}, \quad (7)$$

$$|R|^2 = |R_0|^2\,[1 + A_2^{\,Q}\,m(m+1)]^2 \text{ (for the } Q\text{-branch)}, \quad (8)$$

m being equal to $-J$ in the P-branch, J+1 in the R-branch, and J in the Q-branch. $|R_0|^2$ is the vibrational transition dipole moment squared, and A_1^{PR}, A_2^{PR}, and A_2^{Q}, are Herman-Wallis coefficients. As different formula are used in the literature for the Herman-Wallis factors, it is worth noticing that in the present work the brackets in Eqs. (7) and (8) are squared, and that the bracket in Eq. (8) contains $m(m+1)$, not m^2.

Contrary to what is observed for the forbidden bands studied in Ref. [5], the rotational dependence of $|R|^2$ for the bands studied in the present work can easily be modelled by Eqs. (7) and (8). The list of experimental and calculated line intensities in Supplementary material shows that the observed – calculated residuals are small, namely 2% on the average (see also Table 3), thus showing that the mean precision of the measurements and the efficiency of the model are good. The constants adjusted through unweighted fits of the $|R|^2$ experimental values are listed in Table 4. The most interesting examples of rotational dependences of $|R|^2$ are plotted on Figs. 1-3. Figure 1 shows the $\nu_2 - \nu_5^1$ perpendicular band with its Q-branch. Figure 2 shows the $(2\nu_4 + 2\nu_5)^0_+ - (\nu_4 + \nu_5)^0_+$ band that is a $\Sigma^+_g \leftarrow \Sigma^+_u$ parallel band. Figure 3 shows the strong and opposite rotational dependences observed in the two sub-bands of the ℓ-type doubled $(\nu_4 + 2\nu_5)^1$ I – ν_5^1 parallel band.

The spectra being very crowded, many lines cannot be measured because of blendings with stronger ones. However, this did not prevent from fitting $|R|^2$ experimental values for all the bands. Except for a few cases, we could not measure more lines than those observed by Kabbadj et al. [1]. For the $(2\nu_4 + 2\nu_5)^2$ II – $(\nu_4 + \nu_5)^2$ band at 1318.652 cm^{-1}, many lines of low J value, in the middle of the band, cannot be measured because the ℓ-type doubling is so small that they are unresolved or too overlapped. The uncertainty on line intensities of this band is larger than for the other bands and this has been taken into account when setting up a line list for databases (see next section).

4. Line list for databases

A line list in the HITRAN format has been set up in the same way as in Ref. [5]. As far as line positions are concerned, we have relied on the experimental values of Kabbadj et al. [1]. For lines not observed in Ref. [1], as for a few lines that could be measured in a better way in our spectra, the position obtained by the multispectrum procedure has been taken. For the missing lines and for a few extrapolated ones, positions have been obtained using an effective model based on a polynomial adjustment of experimental line positions.

To generate line intensities, vibrational transition dipole moments squared and Herman-Wallis coefficients (see Table 4) have been used to calculate $|R|^2$ values and then the intensities. As usually done [1,13,14], line intensities corresponding to a few higher values of J (about 5 additional values) have been extrapolated for most of the bands, their uncertainty codes being degraded consequently. To calculate the intensities of these additional lines, $|R|^2$ has been fixed at the value calculated for the highest observed J line in each band.

Other spectroscopic data needed in databases are the same as those already put in the last updates of the databases: air- and self-broadening coefficients, default value for the temperature exponent of air-broadening coefficients, constant value for the air-pressure shifting coefficient, and their accuracies [8,15]. Table 5 summarizes the new data added for the $^{12}C_2H_2$ molecule in the studied spectral region. This line list contains *** transitions and is included in Supplementary material.

5. Conclusion

Absolute intensities have been measured for 467 lines in 9 bands of the $^{12}C_2H_2$ spectrum around 7.7 µm. The Herman-Wallis factor has been used to model the spectrum. A line list containing *** transitions has been set up in the HITRAN format. Merged in the line list set up in Ref. [5], these new data give now a quasi-exhaustive view of the $^{12}C_2H_2$ spectrum in the involved spectral region (an up-to-date full file of *** transitions is also given in Supplementary material). However, one should note that a few series of lines remain unassigned. Furthermore, the set of almost 900 experimental line intensities obtained in Ref. [5] and in the present work can be treated by a global model, as this of Perevalov et al. [16,17]. This model would be able to achieve the assignments and to rigorously take into account the numerous resonances, especially the case of the forbidden bands.

References

[1] Kabbadj Y, Herman M, Di Lonardo G, Fusina L, Johns JWC. The bending energy levels of C_2H_2. J Mol Spectrosc 1991;150:535-65.

[2] Vander Auwera J. Absolute intensities measurements in the $(\nu_4 + \nu_5)$ band of $^{12}C_2H_2$: analysis of Herman-Wallis effects and forbidden transitions. J Mol Spectrosc 2000;201:143-50.

[3] Jacquemart D, Mandin JY, Dana V, Régalia-Jarlot L, Thomas X, Von der Heyden P. Multispectrum fitting measurements of line parameters for 5-µm cold bands of acetylene. JQSRT 2002;75:397-422.

[4] Lepère M, Blanquet G, Walrand J, Bouanich JP, Herman M, Vander Auwera J. Self-broadening coefficients and absolute line intensities in the $\nu_4 + \nu_5$ band of acetylene. J Mol Spectrosc 2007;242:25-30.

[5] Gomez L, Jacquemart D, Lacome N, Mandin JY. Line intensities of $^{12}C_2H_2$ in the 7.7 µm spectral region. JQSRT in press, doi: 10.1016/j.jqsrt.2009.05.018.

[6] El Idrissi MI, Liévin J, Campargue A, Herman M. The vibrational energy pattern in acetylene (IV): updated global vibration constants for $^{12}C_2H_2$. J Chem Phys 1999;110:2074-86.

[7] Matsuura M, Wood PR, Sloan GC, Zijlstra AA. Spitzer observations of acetylene bands in carbon-rich asymptotic giant branch stars in the Large Magellanic Cloud. Mon Not R Astron Soc 2006;371:415-20.

[8] Rothman LS, Gordon IE, Barbe A, Chris Benner D, et al. The HITRAN 2008 Molecular Spectroscopic database. JQSRT 2009;110:533-72.

[9] Jacquinet-Husson N, Scott NA, Chédin A, Garceran K, et al. The 2003 edition of GEISA / IASI spectroscopic database. JQSRT 2005;95:429-67.

[10] Jacquemart D, Mandin JY, Dana V, Picqué N, Guelachvili G. A multispectrum fitting procedure to deduce molecular line parameters. Application to the 3–0 band of $^{12}C^{16}O$. Eur Phys J D 2001;14:55-69.

[11] Jacquemart D, Mandin JY, Dana V, Régalia-Jarlot L, Plateaux JJ, Décatoire D, Rothman LS. The spectrum of acetylene in the 5-µm region from new line-parameter measurements. JQSRT 2003;76:237-67.

[12] Fischer J, Gamache RR, Goldman A, Rothman LS, Perrin A. Total internal partition sums for molecular species in the 2000 edition of the HITRAN database. JQSRT 2003;82:401-12.

[13] Jacquemart D, Lacome N, Mandin JY, Dana V, Tran H, Gueye FK, Lyulin OM, Perevalov VI, Régalia-Jarlot L. The IR spectrum of $^{12}C_2H_2$: line intensity measurements in the 1.4 µm region and update of the databases. JQSRT 2009;110:717-32.

[14] Jacquemart D, Lacome N, Mandin JY. Line intensities of $^{12}C_2H_2$ in the 1.3, 1.2, and 1 µm spectral regions. JQSRT 2009;110:733-42.

[15] Jacquemart D, Lacome N, Mandin JY, Dana V, Lyulin OM, Perevalov VI. Multispectrum fitting procedure for $^{12}C_2H_2$ in the 3.8-μm spectral region. JQSRT 2007;103:478-95.

[16] Perevalov VI, Lobodenko EI, Teffo JL. Reduced effective Hamiltonian for global fitting of C_2H_2 rovibrational lines. In: Proceedings of the XIIth Symposium and School on High-Resolution Molecular Spectroscopy, St. Petersburg. SPIE 1997;3090:143-9.

[17] Perevalov VI, Lyulin OM, Jacquemart D, Claveau C, Teffo JL, Dana V, et al. Global fitting of line intensities of acetylene molecule in the infrared using the effective operator approach. J Mol Spectrosc 2003;218:180–9.

Captions of Tables

Table 1

List of the bands observed by Kabbadj et al. [1] in the $\Delta P = 2$ series of transitions of $^{12}C_2H_2$ around 7.7 µm and studied in this paper.

Table 2

Main experimental conditions of the spectra recorded around 7.7 µm using the rapid-scan interferometer in Paris (LADIR).

Table 3

Line positions and intensities for selected bands of the $^{12}C_2H_2$ molecule in the 7.7 µm region.

Table 4

Summary of $^{12}C_2H_2$ experimental vibrational transition dipole moments squared $|R_0|^2$ in D^2 (1 D = 3.33546×10^{-30} C m), and Herman-Wallis coefficients, see Eqs. (7) and (8), in the 7.7 µm spectral region.

Table 5

Summary of new bands and transitions added at 7.7 µm for the $^{12}C_2H_2$ molecule.

Captions of Figures

Fig. 1. Variation of the transition dipole moment squared $|R|^2$, in D^2 (1 D = 3.33546×10^{-30} C m), vs. *m*, for the $\nu_2 - \nu_5^1$ band. Solid triangles are experimental values obtained in this work for the *P*- and *R*-branches whereas open triangles are for the *Q*-branch. The lines represent the values calculated using the constants reported in Table 4, the solid line being for the *P*- and *R*-branches, and the dashed one for the *Q*-branch.

Fig. 2. Variation of the transition dipole moment squared $|R|^2$, in D^2 (1 D = 3.33546×10^{-30} C m), vs. *m*, for the $(2\nu_4 + 2\nu_5)^0{}_+ - (\nu_4 + \nu_5)^0{}_+$ band. Solid triangles are experimental values obtained in this work. The line represents the values calculated using the constants reported in Table 4.

Fig. 3. Variation of the transition dipole moment squared $|R|^2$, in D^2 (1 D = 3.33546×10^{-30} C m), vs. *m*, for the $(\nu_4 + 2\nu_5)^1$ I $- \nu_5^1$ band. Solid triangles are experimental values obtained in the *e* sub-band, and open ones in the *f* sub-band. The lines represent the values calculated using the constants reported in Table 4. The solid line is for the *e* sub-band, and the dashed one for the *f* sub-band.

Table 1

List of the bands observed by Kabbadj et al. [1] in the $\Delta P = 2$ series of transitions of $^{12}C_2H_2$ around 7.7 µm and studied in this paper.

Band	Center [a]	Upper level [b]	Polyad [b]	Symmetry
$\nu_2 - \nu_5^1$	1245.140	$010(00)^0_+$	$\{3\nu_5\}$	$\Sigma^+_g \leftarrow \Pi_u$
$(\nu_4 + 3\nu_5)^0_+ - 2\nu_5^0$	1308.686	$000(13)^0_+$	$\{4\nu_5\}$	$\Sigma^+_u \leftarrow \Sigma^+_g$
$(\nu_4 + 3\nu_5)^2 - 2\nu_5^2$	1310.182	$000(13)^2$	$\{4\nu_5\}$	$\Delta_u \leftarrow \Delta_g$
$(2\nu_4 + 2\nu_5)^2$ II $- (\nu_4 + \nu_5)^2$	1318.652	$000(22)^2$ II	$\{4\nu_5\}$	$\Delta_g \leftarrow \Delta_u$
$(2\nu_4 + 2\nu_5)^0_+ - (\nu_4 + \nu_5)^0_+$	1319.942	$000(22)^0_+$	$\{4\nu_5\}$	$\Sigma^+_g \leftarrow \Sigma^+_u$
$(2\nu_4 + 2\nu_5)^0_- - (\nu_4 + \nu_5)^0_-$	1320.638	$000(22)^0_-$	$\{4\nu_5\}$	$\Sigma^-_g \leftarrow \Sigma^-_u$
$(3\nu_4 + \nu_5)^2 - 2\nu_4^2$	1328.019	$000(31)^2$	$\{4\nu_5\}$	$\Delta_u \leftarrow \Delta_g$
$(3\nu_4 + \nu_5)^0_+ - 2\nu_4^0$	1330.206	$000(31)^0_+$	$\{4\nu_5\}$	$\Sigma^+_u \leftarrow \Sigma^+_g$
$(\nu_4 + 2\nu_5)^1$ I $- \nu_5^1$	1336.644	$000(12)^1$ I	$\{3\nu_5\}$	$\Pi_g \leftarrow \Pi_u$

[a] Band centers, in cm^{-1}, have been compiled from Ref. [1].
[b] For each band, the upper vibrational level and the polyad to which it belongs have been quoted.

Table 2

Main experimental conditions of the spectra recorded around 7.7 µm using the rapid-scan interferometer in Paris (LADIR).

Commercial sample (Air Liquide Alphagaz)	
Natural C_2H_2	97.760% of $^{12}C_2H_2$
Stated purity	99.55%
Maximum path difference	180 cm
Unapodized FWHM resolution	$\approx 2.8 \times 10^{-3}$ cm^{-1}

Spectrum number	Total pressure (hPa) ±0.5% [a]	Absorbing path (cm) ±1 cm [a]	Temperature (K) ±0.5 K [a]
1	7.585	2015	297.15
2	2.283	2015	296.45
3	1.254	2015	297.15
4	0.8185	2015	297.85
5	0.4283	2015	298.35
6	0.1971	2015	298.95

[a] Absolute uncertainty (excess digits are given as a guide).

Table 3

Line positions and intensities for selected bands of the $^{12}C_2H_2$ molecule in the 7.7 µm region. [a]

Line	Position	S_{obs}	S_{calc}	%	$\|R\|^2_{obs}$
$\nu_2 - \nu_5^1$					
Pee36	1153.23852	3.908E-25	4.119E-25	-5.40	4.227E-04
Pee34	1158.72106	8.876E-25	8.810E-25	0.74	4.497E-04
Pee32	1164.15954	1.710E-24	1.795E-24	-4.97	4.260E-04
Pee30	1169.55603	3.500E-24	3.483E-24	0.49	4.503E-04
Pee29	1172.23791	1.617E-24	1.587E-24	1.86	4.570E-04
Pee28	1174.90942	6.412E-24	6.429E-24	-0.27	4.478E-04
Pee27	1177.56994	2.930E-24	2.858E-24	2.46	4.608E-04
Pee26	1180.21960	1.119E-23	1.129E-23	-0.89	4.460E-04
Pee25	1182.85827	4.929E-24	4.891E-24	0.77	4.538E-04
Pee24	1185.48608	1.876E-23	1.883E-23	-0.37	4.491E-04
Pee23	1188.10290	8.080E-24	7.951E-24	1.60	4.585E-04
Pee22	1190.70861	2.935E-23	2.982E-23	-1.60	4.445E-04
Pee21	1193.30322	1.221E-23	1.226E-23	-0.41	4.501E-04
Pee20	1195.88671	4.534E-23	4.477E-23	1.26	4.582E-04
Pee19	1198.45910	1.817E-23	1.792E-23	1.38	4.593E-04
Pee18	1201.02038	6.405E-23	6.365E-23	0.62	4.562E-04
Pee17	1203.57043	2.686E-23	2.477E-23	7.78	4.921E-04
Pee16	1206.10900	8.429E-23	8.548E-23	-1.41	4.479E-04
Pee15	1208.63647	3.447E-23	3.230E-23	6.30	4.852E-04
Pee14	1211.15234	1.077E-22	1.082E-22	-0.46	4.531E-04
Pee13	1213.65698	3.863E-23	3.962E-23	-2.56	4.442E-04
Pee12	1216.15014	1.247E-22	1.284E-22	-2.97	4.428E-04
Pee11	1218.63195	4.435E-23	4.546E-23	-2.50	4.453E-04
Pee11	1218.63195	4.435E-23	4.546E-23	-2.50	4.453E-04
Pee 9	1223.56066	4.978E-23	4.846E-23	2.65	4.698E-04
Pee 8	1226.00781	1.439E-22	1.454E-22	-1.04	4.529E-04
Pee 6	1230.86694	1.339E-22	1.351E-22	-0.90	4.546E-04
Pee 4	1235.67919	1.130E-22	1.101E-22	2.57	4.717E-04
Pee 3	1238.06762	3.175E-23	3.082E-23	2.93	4.739E-04
Pee 2	1240.44433	7.297E-23	7.197E-23	1.37	4.668E-04
Pee 1	1242.80920	1.609E-23	1.641E-23	-1.99	4.518E-04
Qef27	1237.11706	1.858E-23	1.849E-23	0.48	4.798E-04
Qef26	1237.69018	7.839E-24	8.077E-24	-3.04	4.623E-04
Qef25	1238.24231	3.178E-23	3.135E-23	1.35	4.817E-04
Qef24	1238.77331	1.348E-23	1.335E-23	0.96	4.788E-04
Qef23	1239.28332	4.974E-23	5.049E-23	-1.51	4.661E-04
Qef21	1240.24011	7.758E-23	7.711E-23	0.61	4.740E-04
Qef20	1240.68676	3.126E-23	3.114E-23	0.38	4.721E-04
Qef18	1241.51684	4.391E-23	4.382E-23	0.20	4.695E-04
Qef17	1241.90002	1.541E-22	1.527E-22	0.91	4.721E-04
Qef16	1242.26220	5.852E-23	5.826E-23	0.44	4.692E-04
Qef15	1242.60302	1.967E-22	1.970E-22	-0.15	4.657E-04
Qef14	1242.92260	7.242E-23	7.288E-23	-0.64	4.628E-04
Qef13	1243.22094	2.424E-22	2.388E-22	1.49	4.721E-04
Qef10	1243.98852	9.292E-23	9.335E-23	-0.46	4.615E-04
Qef 9	1244.20178	2.823E-22	2.840E-22	-0.60	4.605E-04
Qef 6	1244.71386	8.566E-23	8.516E-23	0.58	4.649E-04
Qef 5	1244.84179	2.238E-22	2.315E-22	-3.44	4.466E-04

Table 3 (continued)

Line	Position	S_{obs}	S_{calc}	%	$\|R\|^2_{obs}$
Qef 4	1244.94860	6.706E-23	6.685E-23	0.31	4.632E-04
Qef 3	1245.03393	1.612E-22	1.632E-22	-1.24	4.558E-04
Qef 2	1245.09802	4.060E-23	4.022E-23	0.94	4.658E-04
Qef 1	1245.14074	7.471E-23	7.406E-23	0.87	4.654E-04
Ree 1	1249.83190	8.060E-24	8.276E-24	-2.68	4.501E-04
Ree 2	1252.14880	4.847E-23	4.867E-23	-0.41	4.607E-04
Ree 3	1254.45361	2.306E-23	2.358E-23	-2.25	4.528E-04
Ree 4	1256.74646	8.551E-23	9.037E-23	-5.68	4.386E-04
Ree 4	1256.74646	8.551E-23	9.037E-23	-5.68	4.386E-04
Ree 6	1261.29541	1.213E-22	1.202E-22	0.91	4.687E-04
Ree 7	1263.56250	4.349E-23	4.327E-23	0.51	4.672E-04
Ree 8	1265.79553	1.403E-22	1.357E-22	3.28	4.809E-04
Ree 9	1268.02722	4.637E-23	4.606E-23	0.67	4.689E-04
Ree10	1270.24646	1.400E-22	1.373E-22	1.93	4.754E-04
Ree14	1278.99951	1.129E-22	1.097E-22	2.83	4.816E-04
Ree15	1281.15661	3.353E-23	3.310E-23	1.28	4.745E-04
Ree16	1283.30114	8.863E-23	8.845E-23	0.20	4.698E-04
Ree21	1293.83361	1.319E-23	1.324E-23	-0.38	4.693E-04
Ree22	1295.90210	3.176E-23	3.245E-23	-2.17	4.615E-04
Ree26	1304.04650	1.291E-23	1.265E-23	2.01	4.829E-04
Ree28	1308.04113	7.176E-24	7.311E-24	-1.88	4.655E-04
$(2\nu_4 + 2\nu_5)^0_+ - (\nu_4 + \nu_5)^0_+$					
Pee32	1246.08773	7.277E-24	7.393E-24	-1.59	1.622E-02
Pee31	1248.42957	3.470E-24	3.455E-24	0.43	1.660E-02
Pee30	1250.76645	1.376E-23	1.436E-23	-4.36	1.588E-02
Pee29	1253.09876	6.537E-24	6.546E-24	-0.14	1.659E-02
Pee26	1260.06462	4.661E-23	4.654E-23	0.15	1.675E-02
Pee25	1262.37582	2.000E-23	2.015E-23	-0.75	1.663E-02
Pee22	1269.27837	1.240E-22	1.225E-22	1.21	1.704E-02
Pee20	1273.85700	1.883E-22	1.834E-22	2.60	1.733E-02
Pee19	1276.14089	7.434E-23	7.318E-23	1.56	1.716E-02
Pee16	1282.97960	3.515E-22	3.457E-22	1.65	1.721E-02
Pee14	1287.53642	4.424E-22	4.333E-22	2.06	1.729E-02
Pee13	1289.81693	1.604E-22	1.578E-22	1.62	1.721E-02
Pee12	1292.09992	5.066E-22	5.079E-22	-0.26	1.689E-02
Pee11	1294.38634	1.789E-22	1.784E-22	0.28	1.698E-02
Pee10	1296.67696	5.598E-22	5.527E-22	1.27	1.714E-02
Pee 8	1301.27379	5.456E-22	5.511E-22	-1.01	1.673E-02
Pee 7	1303.58127	1.760E-22	1.764E-22	-0.23	1.685E-02
Pee 6	1305.89550	4.846E-22	4.915E-22	-1.42	1.663E-02
Pee 5	1308.21694	1.458E-22	1.464E-22	-0.41	1.678E-02
Pee 3	1312.88268	9.777E-23	9.748E-23	0.30	1.685E-02
Pee 2	1315.22747	2.026E-22	2.018E-22	0.39	1.684E-02
Pee 1	1317.58032	3.489E-23	3.442E-23	1.35	1.697E-02
Ree 0	1322.31021	1.054E-22	1.044E-22	0.95	1.684E-02
Ree 1	1324.68698	6.956E-23	6.876E-23	1.15	1.683E-02
Ree 2	1327.07135	2.956E-22	3.023E-22	-2.27	1.623E-02
Ree 3	1329.46299	1.314E-22	1.297E-22	1.29	1.677E-02
Ree 4	1331.86139	4.587E-22	4.642E-22	-1.20	1.631E-02

Table 3 (continued)

Line	Position	S_{obs}	S_{calc}	%	$\|R\|^2_{obs}$
Ree 6	1336.67656	5.629E-22	5.712E-22	-1.47	1.617E-02
Ree 8	1341.51145	6.039E-22	6.168E-22	-2.14	1.596E-02
Ree 9	1343.93448	2.033E-22	2.056E-22	-1.13	1.606E-02
Ree10	1346.35999	5.921E-22	6.037E-22	-1.96	1.587E-02
Ree11	1348.78706	1.914E-22	1.932E-22	-0.94	1.597E-02
Ree12	1351.21461	5.506E-22	5.460E-22	0.84	1.619E-02
Ree13	1353.64167	1.680E-22	1.684E-22	-0.24	1.595E-02
Ree14	1356.06711	4.534E-22	4.600E-22	-1.46	1.569E-02
Ree15	1358.48994	1.375E-22	1.373E-22	0.15	1.587E-02
Ree16	1360.90913	3.587E-22	3.633E-22	-1.28	1.557E-02
Ree17	1363.32367	1.058E-22	1.052E-22	0.57	1.578E-02
Ree18	1365.73258	2.736E-22	2.702E-22	1.24	1.581E-02
Ree19	1368.13538	7.583E-23	7.599E-23	-0.21	1.550E-02
Ree20	1370.53106	1.871E-22	1.897E-22	-1.39	1.524E-02
Ree22	1375.29924	1.236E-22	1.260E-22	-1.94	1.498E-02
Ree23	1377.67095	3.340E-23	3.354E-23	-0.42	1.512E-02
Ree24	1380.03414	7.860E-23	7.935E-23	-0.95	1.495E-02
Ree25	1382.38877	2.115E-23	2.057E-23	2.74	1.542E-02
Ree26	1384.73478	4.750E-23	4.737E-23	0.27	1.494E-02
Ree27	1387.07250	1.208E-23	1.197E-23	0.91	1.494E-02
Ree28	1389.40185	2.712E-23	2.686E-23	0.96	1.484E-02
Ree30	1394.03709	1.448E-23	1.448E-23	0.00	1.449E-02
Ree31	1396.34345	3.547E-24	3.478E-24	1.95	1.467E-02
$(\nu_4 + 2\nu_5)^1$ I – ν_5^1					
Pee29	1274.86923	3.864E-24	4.042E-24	-4.61	3.003E-05
Pee27	1278.69290	6.840E-24	6.767E-24	1.07	2.971E-05
Pee26	1280.62930	2.573E-23	2.580E-23	-0.27	2.838E-05
Pee25	1282.58202	1.078E-23	1.079E-23	-0.09	2.753E-05
Pee22	1288.53764	6.335E-23	5.936E-23	6.30	2.682E-05
Pee20	1292.58947	8.721E-23	8.345E-23	4.31	2.478E-05
Pee16	1300.88758	1.391E-22	1.404E-22	-0.93	2.110E-05
Pee15	1303.00244	5.181E-23	5.146E-23	0.68	2.092E-05
Pee13	1307.28039	6.173E-23	5.940E-23	3.77	2.061E-05
Pee10	1313.81747	1.890E-22	1.946E-22	-2.96	1.810E-05
Pee 9	1316.02852	6.367E-23	6.420E-23	-0.83	1.814E-05
Pee 8	1318.25530	1.834E-22	1.861E-22	-1.47	1.771E-05
Pee 7	1320.49808	5.765E-23	5.836E-23	-1.23	1.747E-05
Pee 5	1325.03106	4.720E-23	4.620E-23	2.12	1.755E-05
Pee 4	1327.32120	1.062E-22	1.134E-22	-6.78	1.589E-05
Ree 1	1341.39131	1.614E-23	1.615E-23	-0.06	1.616E-05
Ree 2	1343.79080	8.298E-23	8.404E-23	-1.28	1.591E-05
Ree 4	1348.63612	1.417E-22	1.398E-22	1.34	1.629E-05
Ree 5	1351.08193	5.220E-23	5.363E-23	-2.74	1.566E-05
Ree 6	1353.54297	1.751E-22	1.774E-22	-1.31	1.592E-05
Ree 8	1358.51097	1.933E-22	1.960E-22	-1.40	1.604E-05
Ree 9	1361.01783	6.988E-23	6.620E-23	5.27	1.728E-05
Ree10	1363.53974	1.953E-22	1.970E-22	-0.87	1.635E-05
Ree11	1366.07680	6.422E-23	6.398E-23	0.37	1.671E-05
Ree13	1371.19607	5.796E-23	5.765E-23	0.53	1.711E-05
Ree16	1378.98706	1.318E-22	1.320E-22	-0.15	1.773E-05

Table 3 (continued)

Line	Position	S_{obs}	S_{calc}	%	$\|R\|^2_{obs}$
Ree18	1384.25512	1.060E-22	1.028E-22	3.02	1.895E-05
Ree19	1386.91121	2.972E-23	2.965E-23	0.24	1.877E-05
Ree20	1389.58197	7.707E-23	7.598E-23	1.41	1.938E-05
Ree21	1392.26721	2.141E-23	2.136E-23	0.23	1.956E-05
Ree22	1394.96700	5.341E-23	5.338E-23	0.06	1.996E-05
Ree23	1397.68116	1.470E-23	1.465E-23	0.34	2.049E-05
Ree24	1400.40980	3.633E-23	3.572E-23	1.68	2.127E-05
Ree25	1403.15269	9.584E-24	9.561E-24	0.24	2.149E-05
Ree26	1405.90973	2.337E-23	2.276E-23	2.61	2.259E-05
Ree27	1408.68082	6.489E-24	5.950E-24	8.31	2.464E-05
Ree29	1414.26583	3.436E-24	3.530E-24	-2.74	2.325E-05
Ree30	1417.07907	7.800E-24	8.018E-24	-2.79	2.392E-05
Ree31	1419.90641	1.903E-24	1.999E-24	-5.04	2.411E-05
Pff23	1281.84536	1.572E-23	1.718E-23	-9.29	8.319E-06
Pff19	1291.43217	4.709E-23	4.656E-23	1.13	1.122E-05
Pff16	1298.60958	2.795E-23	2.734E-23	2.18	1.274E-05
Pff15	1300.99923	9.663E-23	9.553E-23	1.14	1.303E-05
Pff14	1303.38738	3.724E-23	3.642E-23	2.20	1.358E-05
Pff13	1305.77427	1.232E-22	1.226E-22	0.49	1.373E-05
Pff12	1308.15926	4.474E-23	4.497E-23	-0.51	1.395E-05
Pff10	1312.92452	5.059E-23	5.102E-23	-0.85	1.455E-05
Pff 9	1315.30456	1.570E-22	1.574E-22	-0.25	1.492E-05
Pff 8	1317.68284	5.281E-23	5.255E-23	0.49	1.530E-05
Pff 7	1320.05919	1.561E-22	1.529E-22	2.05	1.578E-05
Pff 6	1322.43379	4.784E-23	4.772E-23	0.25	1.571E-05
Pff 5	1324.80638	1.259E-22	1.279E-22	-1.59	1.561E-05
Pff 4	1327.17700	3.564E-23	3.568E-23	-0.11	1.599E-05
Pff 3	1329.54570	7.876E-23	8.042E-23	-2.11	1.580E-05
Rff 1	1341.35664	4.735E-23	4.894E-23	-3.36	1.580E-05
Rff 3	1346.06565	1.140E-22	1.151E-22	-0.96	1.605E-05
Rff 4	1348.41662	4.669E-23	4.667E-23	0.04	1.611E-05
Rff 7	1355.45502	1.762E-22	1.822E-22	-3.41	1.510E-05
Rff 8	1357.79628	6.078E-23	6.181E-23	-1.69	1.514E-05
Rff 9	1360.13506	1.812E-22	1.837E-22	-1.38	1.495E-05
Rff10	1362.47132	5.769E-23	5.921E-23	-2.63	1.450E-05
Rff11	1364.80485	1.698E-22	1.680E-22	1.06	1.474E-05
Rff12	1367.13591	5.270E-23	5.186E-23	1.59	1.450E-05
Rff13	1369.46442	1.401E-22	1.414E-22	-0.93	1.380E-05
Rff14	1371.79030	4.149E-23	4.199E-23	-1.21	1.340E-05
Rff17	1378.75178	7.915E-23	7.999E-23	-1.06	1.221E-05
Rff18	1381.06674	2.271E-23	2.213E-23	2.55	1.221E-05
Rff20	1385.68889	1.479E-23	1.449E-23	2.03	1.119E-05
Rff21	1387.99583	3.483E-23	3.428E-23	1.58	1.064E-05
Rff22	1390.29990	8.538E-24	8.866E-24	-3.84	9.604E-06
Rff24	1394.89974	4.991E-24	5.072E-24	-1.62	8.802E-06
Rff25	1397.19562	1.187E-23	1.121E-23	5.56	8.914E-06
Rff28	1404.06505	1.259E-24	1.348E-24	-7.07	6.376E-06
Rff29	1406.35000	2.988E-24	2.777E-24	7.06	6.777E-06

[a] The quoted line position is this measured in this work, in cm^{-1}. S_{obs} and S_{calc} are measured and calculated intensities, respectively, for pure $^{12}C_2H_2$ (i.e., for a sample containing 100% of $^{12}C_2H_2$), in cm molecule^{-1} at 296 K. % is the ratio $100 \times (S_{obs} - S_{calc}) / S_{obs}$. $|R|^2_{obs}$ is the experimental transition dipole moment squared value, in D^2 (1 D = 3.33546×10^{-30} C m), deduced from S_{obs} using Eqs. (1)-(6). Values of $|R|^2_{obs}$ for these bands are illustrated on Figs. 1-3.

Table 4

Summary of $^{12}C_2H_2$ experimental vibrational transition dipole moments squared $|R_0|^2$ in D^2 (1 D = 3.33546 × 10^{-30} C m), and Herman-Wallis coefficients, see Eqs. (7) and (8), in the 7.7 μm spectral region. [a]

Band	Origin	$\|R_0\|^2$	A_1^{PR}	A_2^{PR}
$\nu_2 - \nu_5^1$	1245.140	$4.613(31)\times10^{-4}$	$+4.8(20)\times10^{-4}$	$A_2^Q = +2.3(15)\times10^{-5}$
$(\nu_4 + 3\nu_5)^0_+ - 2\nu_5^0$	1308.686	$1.1586(77)\times10^{-2}$	$-1.66(25)\times10^{-3}$	$-3.6(13)\times10^{-5}$
$(\nu_4 + 3\nu_5)^2 - 2\nu_5^2$	1310.182	$2.170(16)\times10^{-2}$	e $-1.55(26)\times10^{-3}$	
			f $-1.40(30)\times10^{-3}$	
$(2\nu_4 + 2\nu_5)^2$ II $- (\nu_4 + \nu_5)^2$	1318.652	$2.127(29)\times10^{-2}$	e $-1.59(33)\times10^{-3}$	
			f $-1.81(52)\times10^{-3}$	$-4.11(26)\times10^{-4}$
$(2\nu_4 + 2\nu_5)^0_+ - (\nu_4 + \nu_5)^0_+$	1319.942	$1.6709(99)\times10^{-2}$	$-1.02(11)\times10^{-3}$	$-3.86(62)\times10^{-5}$
$(2\nu_4 + 2\nu_5)^0_- - (\nu_4 + \nu_5)^0_-$	1320.638	$1.147(22)\times10^{-2}$	$-2.26(71)\times10^{-3}$	$-5.89(60)\times10^{-4}$
$(3\nu_4 + \nu_5)^2 - 2\nu_4^2$	1328.019	$2.074(21)\times10^{-2}$	e $-4.5(27)\times10^{-4}$	$+2.7(14)\times10^{-5}$
			f $-1.30\ (29)\times10^{-3}$	
$(3\nu_4 + \nu_5)^0_+ - 2\nu_4^0$	1330.206	$1.035(11)\times10^{-2}$	$-1.77(26)\times10^{-3}$	$-1.3(15)\times10^{-5}$
$(\nu_4 + 2\nu_5)^1$ I $- \nu_5^1$	1336.644	$1.634(19)\times10^{-5}$	e $-3.35(24)\times10^{-3}$	$+3.44(15)\times10^{-4}$
			f $+7.7(51)\times10^{-4}$	$-4.47(28)\times10^{-4}$

[a] 95% confidence intervals (2 SD, in unit of the last quoted digit) are given between parenthesis. For $|R_0|^2$ values, the overall accuracy is 5% on the mean. Non given Herman-Wallis coefficients have been fixed at zero.

Table 5

Summary of new bands and transitions added at 7.7 µm for the $^{12}C_2H_2$ molecule. [a]

Band	Origin	ν_{min} - ν_{max}	ΣS	S_{min} - S_{max}	$J_{max}\nu$ /	$J_{max}S$ /	J_{max}	Cdν	CdS
000220–_–000112	1311.31	1288-1377	1.9E-21	1.0E-25-6.4E-22	13-23	13-23	13-23	4/2	5/3
**** format ****									
010000+_–000011__	1245.140				36-28	36-28		4/3	6/5
					27	27		4/3	6/5
000130+_–000020+_	1308.686				29-16	29-16		4/3	6/5
000132__–000022__	1310.182				31-27	28-27		4/3	6/5
000222_2–000112__	1318.652				32-30	32-30		3/2	5/4
000220+_–000110+_	1319.942				32-31	32-31		4/3	6/5
000220–_–000110–_	1320.638				25-15	23-14		4/3	6/5
000312__–000202__	1328.019				31-33	31-33		4/3	6/5
000310+_–000200+_	1330.206				31-29	29-29		4/3	6/5
000121_1–000011__	1336.644				29-31	29-31		4/3	6/5

[a] Explanation of the column headings:
Band: vibrational assignment used in the line list, according to Section 1: v_1 v_2 v_3 v_4 v_5 $\ell \pm r$ for the upper and lower states. When ± or r does not occur for the upper state, it is replaced by an underscore. Note that r is mentionned only if necessary to avoid ambiguities.
Origin: approximate value of the band center, in cm^{-1}.
ν_{min} - ν_{max} : limiting values of line positions, in cm^{-1}.
ΣS : sum of line intensities, in cm $molecule^{-1}$ at 296 K.
S_{min} - S_{max} : limiting values of line intensities, in cm $molecule^{-1}$ at 296 K.
$J_{max}\nu$: maximum value of J for which a line position has been measured.
$J_{max}S$: maximum value of J for which a line intensity has been measured.
J_{max} : maximum value of J present in the line list.
(The first value is for the P-branch and the second for the R-branch. When a value is on a separate line, it concerns the Q-branch of the above band.)
Cdν: uncertainty code for line positions [8]:
Code 2: 10^{-2}-10^{-1} cm^{-1}. Code 3: 10^{-3}-10^{-2} cm^{-1}. Code 4: 10^{-4}-10^{-3} cm^{-1}.
CdS: uncertainty code for line intensities [8]:
Code 4: 10-20%. Code 5: 5-10%. Code 6: 2-5%.
(The second value is for some interpolated or extrapolated lines.)
Other spectroscopic data are the same as those already put in the last updates of the databases: air- and self-broadening coefficients, default value for the temperature exponent of air-broadening coefficients, constant value for the air-pressure shifting coefficient, and their accuracies [8,15].

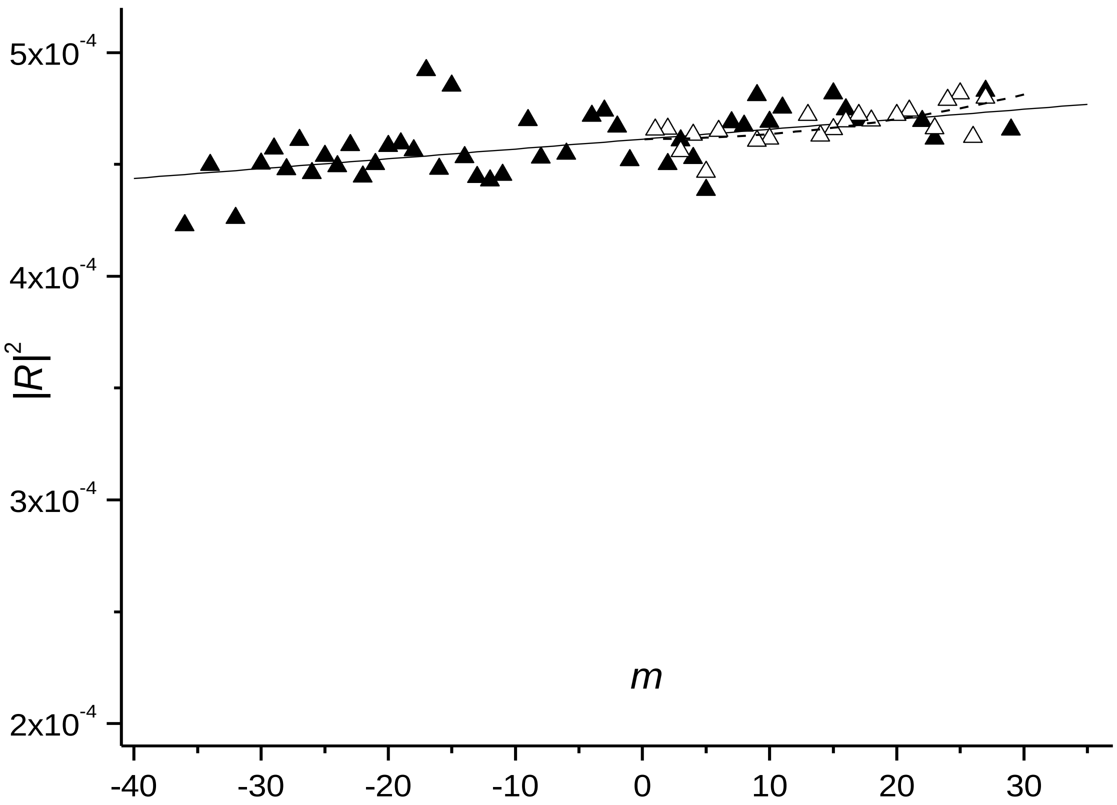

Fig. 1. Variation of the transition dipole moment squared $|R|^2$, in D^2 (1 D = 3.33546 × 10^{-30} C m), vs. m, for the $\nu_2 - \nu_5^1$ band. Solid triangles are experimental values obtained in this work for the *P*- and *R*-branches whereas open triangles are for the *Q*-branch. The lines represent the values calculated using the constants reported in Table 4, the solid line being for the *P*- and *R*-branches, and the dashed one for the *Q*-branch.

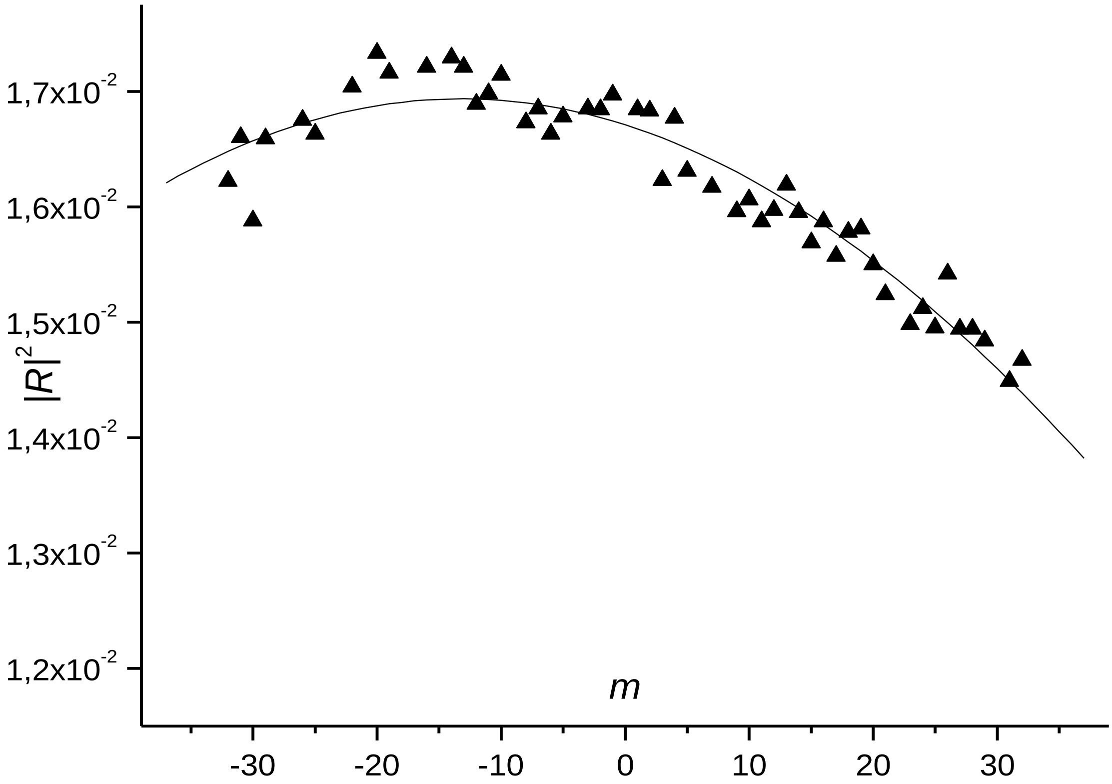

Fig. 2. Variation of the transition dipole moment squared $|R|^2$, in D^2 (1 D = 3.33546 × 10^{-30} C m), vs. *m*, for the $(2\nu_4 + 2\nu_5)^0_+ - (\nu_4 + \nu_5)^0_+$ band. Solid triangles are experimental values obtained in this work. The line represents the values calculated using the constants reported in Table 4.

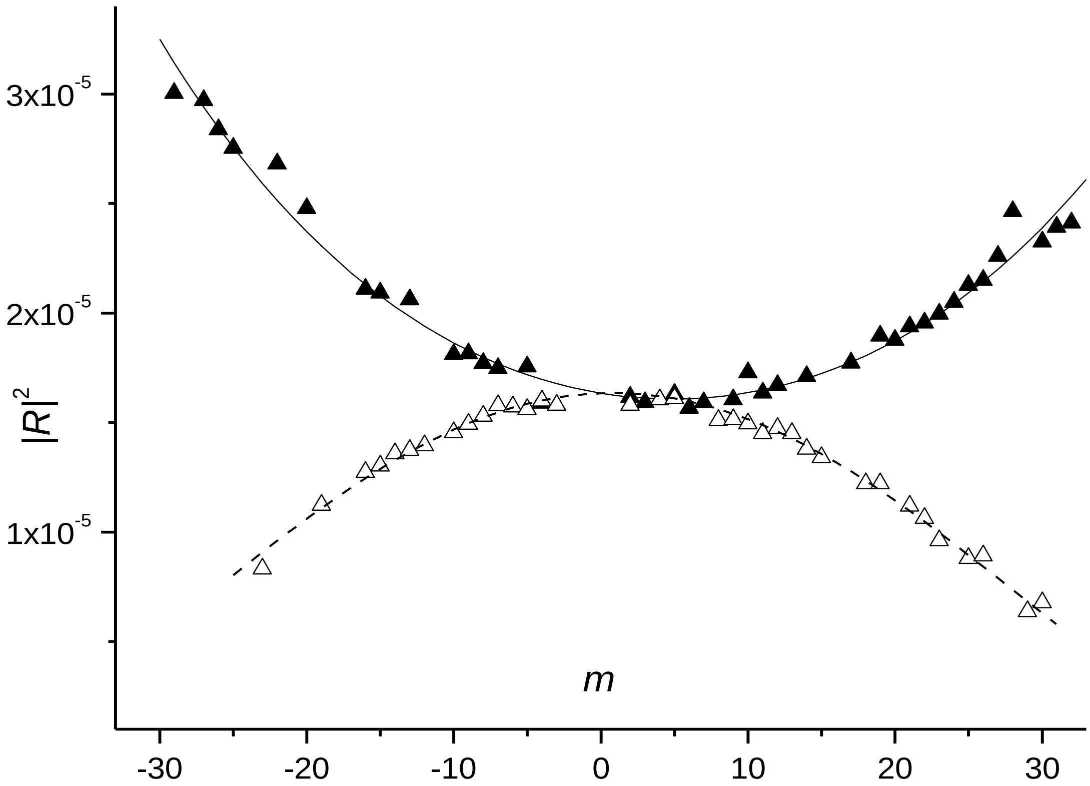

Fig. 3. Variation of the transition dipole moment squared $|R|^2$, in D^2 (1 D = 3.33546×10^{-30} C m), vs. *m*, for the $(\nu_4 + 2\nu_5)^1$ I – ν_5^1 band. Solid triangles are experimental values obtained in the *e* sub-band, and open ones in the *f* sub-band. The lines represent the values calculated using the constants reported in Table 4. The solid line is for the *e* sub-band, and the dashed one for the *f* sub-band.